Structures 65 (2024) 106676

Contents lists available at ScienceDirect

Structures

journal homepage: www.elsevier.com/locate/structures

Effects of passive confinement on out-of-plane robustness of unreinforced masonry infill walls

Sujan Pradhan [a], Yasushi Sanada [b,*], Yoon Rokhyun [b], Ho Choi [c], Kiwoong Jin [d]

[a] Institute of Innovative Research, Tokyo Institute of Technology, Japan
[b] Graduate School of Engineering, Osaka University, Japan
[c] School of Science and Engineering, Shizuoka Institute of Science and Technology, Japan
[d] School of Science and Technology, Meiji University, Japan

ARTICLE INFO

Keywords:
Incremental dynamic test
Infill wall
Lateral resistance
Moment-resistance frame
Safety assessment
Seismic performance
Static tilting test

ABSTRACT

Unreinforced masonry (URM) walls are vulnerable to out-of-plane (OOP) collapse under lateral loads; however, URM structures are still popular in developing countries. Even in many countries classified as developed by the United Nations, URM walls are still commonly applied as exterior and interior infills in engineered buildings, resulting in severe OOP failure during strong earthquakes. The objectives of this study were: 1) to experimentally examine the OOP behavior and performance of URM infills with construction deficiencies commonly found in Asian countries, 2) to investigate the impact of construction quality on resistance to OOP collapse and 3) to propose a promising approach using passive confinement to improve the lateral resistance of URM infills and a method to evaluate their seismic performance. To attain these objectives, the study used two full-scale, single wythe, brick masonry specimens with specific boundary conditions at the top, a control specimen representing URM infills with construction flaws frequently found in Asian countries and a well-constructed specimen subjected to passive confinement under lateral excitation. A series of incremental dynamic shaking table tests was performed on both specimens under OOP unidirectional one-way bending. The test results revealed the positive effects of construction with passive confinement on OOP performance. The results indicated that the OOP robustness of infills can be improved without specific retrofit materials, leading to advantages such as simplicity, cost-effectiveness, and swift execution. Moreover, a theoretical method to evaluate the lateral resistance of infills was presented and verified for practical applications. This method can contribute to reducing the potential for earthquake damage in engineered buildings.

1. Introduction

Unreinforced brick masonry (URM) is one of the oldest building members still in use, even in countries with a high risk of earthquakes. The major cause of fatalities during a seismic event is usually the collapse of weaker seismic components such as URM walls. Hence, some developed countries, including Japan, have imposed certain restrictions on the use of URM walls because of their vulnerability [1]. However, numerous advantages associated with URM have made it an almost unavoidable building element. As a result, URMs are frequently used as infill in frame buildings in many countries [2], including some countries classified as developed by the United Nations. Since the in-plane (IP) performance of infills has a direct influence on building performance by providing additional paths for transferring seismic loads, there have been many studies to investigate the IP performance of infills [3–5]. However, URM infills are weak under tension, which restricts their flexural strength and makes them highly susceptible to out-of-plane (OOP) collapse under lateral loads. As a result, OOP collapse of URM infills is frequently reported during earthquakes [1,6,7]. The collapse of URM infills has dire consequences for the safety and lives of citizens, building functionality, economic loss, and anticipated performance of buildings. Nevertheless, the OOP performance of URM infills is a secondary focus because of its indirect effect on building performance. Moreover, in developing Asian countries, it is common to find construction defects in URM infills, which may make them more vulnerable to OOP collapse. However, the fact was not focused in the past studies. Hence, detailed studies are required to investigate the OOP behavior and performance of URM infills for safety and accurate evaluation of seismic

* Corresponding author.
E-mail address: sanada@arch.eng.osaka-u.ac.jp (Y. Sanada).

https://doi.org/10.1016/j.istruc.2024.106676
Received 30 August 2023; Received in revised form 7 May 2024; Accepted 29 May 2024
Available online 4 June 2024

performance of buildings with infills.

Penner and Elwood [8] performed an OOP shaking table test on URM walls focusing on the effect of diaphragm flexibility. Five full-scale unreinforced brick wall specimens representing load bearing URM buildings were prepared. The specimen with a flexible top diaphragm and rigid bottom diaphragm effectively exhibited no rocking until collapse. Vaculik and Griffith [9] investigated five half-scale URM under the OOP dynamic test via shaking table. Three specimens had a window opening, and three were subjected to vertical precompression. The initial cracking and peak strength reached at low displacements which was consistent with quasistatic cyclic tests and airbag tests reported in the past studies. The study concluded that, independent to the presence or absence of the opening, the precompression increases the OOP strength. The study also predicted a theoretical capacity envelope of the specimens that provided a conservative estimation of the post-cracking strength. Sharma et al. [10] presented the results of incremental dynamic tests on four full-scale URM walls with weak masonry mortar under two-way bending excitation in the OOP direction. Specimens were tested with two boundary conditions; first, two specimens were restrained in both vertical edges and the bottom edge keeping the top edge free and unloaded; second, the remaining specimens were restrained in one vertical and the bottom edge. All the specimens exhibited very brittle behavior and dissipated negligible energy regardless of the boundary conditions. Peng et al. [11] performed a quasi-static test on four infilled frames with rigid or flexible connections between frames and infills and a bare frame. The experimental investigation revealed that the rigid connection increases the strength and stiffness than the flexible connection. On the other hand, it was also found that the connection type did not have a consistent influence on energy dissipation. Erdem et al. [12] used five 2/3 scale RC specimens out of which three were with different flexible connections between frame and infill, one with rigid connection, and one bare frame. The study revealed that all specimens with flexible connections showed IP performance similar to the bare frames up to 2 % drift and infill was undamaged up to 4 % drift. In contrast, the specimen with the rigid connection reached higher strength at a small drift and was significantly damaged. Walsh et al. [13] conducted experimental and analytical studies to investigate the effects of IP shear damage and boundary restraint conditions on the OOP behavior of infills. A total of nineteen tests were performed on sixteen different walls in situ in six different buildings using airbags. The wall configurations had a wide range of geometries, boundary conditions, pre-test damage states, and material properties. The study revealed that IP damage reduces the OOP capacity of a URM infill by up to 40 %. Restraining the vertical edges of the infill results in two-way OOP flexure and improves OOP capacity compared to unrestrained vertical edges. Furthermore, the boundary restraints of the infill from the bounded building frame significantly increases the OOP capacity of the infill. Morandi [14] reported the IP and OOP response of full-scale, single-story, single-bay RC frame infilled with strong URM infill specimens under OOP static cyclic tests. OOP cyclic static tests were performed after IP cyclic tests. The test result revealed a sharp degradation of OOP stiffness after a small IP drift leading to damage initiation and detachment of the infill from the surrounding frame. The study revealed that the behavior factor of infill decreases, while the OOP fundamental period increases as the imposed IP drifts increase. Di Domenico et al. [15] performed experiments on three 2/3 scaled infilled RC frames to assess the impact of IP and OOP interaction on the OOP response of infills and proposed empirical equations for the evaluation of OOP strength and stiffness reduction due to the interaction. One specimen was subjected to pure OOP loading, whereas the remaining two specimens were first subjected to IP cyclic loads up to two different drift levels (0.69 % and 1.03 %) and then subsequently tested under OOP loads. The study revealed that the previous IP loading decreased the OOP strength and stiffness. The study also concluded that the proposed empirical equations can be used to model the OOP performance of infills and for their safety assessment. Milanesi et al. [16] performed an OOP dynamic test on full-scale single-story, single-bay RC frame specimens without and with a central opening on infill via shaking table test that has sustained a certain level of damage due to an IP pseudo-static cyclic tests. Although the specimens were subjected to IP cyclic tests, the infills did not show any significant damage up to a substantial level of acceleration. Due to the shorter span and the more rigid behavior of the infill panel with opening, the panel attained higher acceleration and lower peak displacement than the infill panel without opening. The horizontal-deformed shape of the infill panel with opening resembles a cantilever beam, whereas the one without opening was similar to a simply supported beam. Moreover, the study also investigated a simplified numerical model of infill without opening and evaluated bending moments and damage conditions. The model had good agreement with the experimental results. Jin et al. [17] performed a series of bidirectional quasi-static tests on two types of isolated infilled frames of 1/2 scale single-story, single-bay masonry infilled RC frames to investigate the IP and OOP interactions of the infills. Specimens were first loaded in the IP direction up to two different drifts (2 % and 3 %) and then loaded with OOP loads. The study showed that crack/damage caused by IP loading affects OOP cracking patterns, arching action formation and the reduction of OOP strength (from 20.3 % to 66.1 %) depending on the previous IP drift level. Milijas et al. [18] conducted experimental studies on nine full-scale infilled RC frames with and without openings subjected to pure, sequential, and simultaneous IP and OOP loading. The study revealed that IP and OOP combined loading has a limited effect on the IP response of infill. In contrast, a significant reduction in OOP stiffness and capacity was observed due to previously applied IP loading; specifically, the OOP capacities were reduced approximately by 2 times and 3.7 times for infilled frame without and with opening respectively. Hence, it is most likely to anticipate severe seismic vulnerability of infill with openings when subjected to combined IP and OOP loading. Choi et al. [19] used four 1/4 scale, single-story, single-bay masonry infilled RC frame specimens with and without tie systems (3 types) proposed in the study to upgrade the seismic performance of the infills. Two series of tests were performed; the first series was to compare the fundamental OOP performance of the specimens and the second series was to verify the effectiveness of the full-length tie system. Each series consisted of sequentially IP static cyclic loading and OOP dynamic loading. The study revealed that the tie systems caused a minor effect on the IP performance, and the full-length tie system significantly reduced the infill damage and prevented the OOP collapse of the infill. Baek et al. [20] performed a series of shaking table tests on a 60 % scaled two-story non-seismically designed infilled RC building. The tests used simultaneous loading in two directions to investigate the effect of different types of openings, and the combined effect of IP and OOP damage mechanisms. The study revealed that infills without openings collapsed due to IP diagonal cracking and OOP inclination, while infills with openings collapsed subsequently due to considerable rotation, and cracking that initiated from the opening corners. The OOP collapse of the infill can be accelerated because of the degradation of the infill-frame boundary due to IP displacements. The study also concluded that the higher story infills of non-seismically designed buildings are more vulnerable when simultaneously subjected to IP and OOP loads. Moreover, several codes, such as Eurocode 6 [21], FEMA-306 [22] and NZSEE [23], provide equations to estimate the OOP strength of infill walls. A comparative study conducted by Gesualdi et al. [24] revealed that using Eurocode 6 [21] overestimated OOP strength, while using FEMA-306 [22] and NZSEE [23] significantly underestimated OOP strength. Furthermore, several past studies [25–29] have investigated the OOP performance of URM infill walls. However, no detailed studies on the OOP performance of URM infill with an improper construction quality, commonly found in developing countries, have been conducted till date.

URM infills are usually constructed after reinforced concrete (RC) frames are cast, creating difficulties in filling mortar between the top infill layer and the bottom surface of the upper beam or slab, resulting in

improper filling at the top. This represents improper construction quality of the infill but common in developing countries, as shown in Fig. 1. Nevertheless, the consequences of the aforementioned improper construction quality on OOP performance of infill walls have yet to be addressed. Thus, in light of the actual construction practice of URM infills and the limitations of past studies, this paper discusses 1) the characteristics of URM infills commonly observed in developing Asian countries and their behavior and performance under lateral loads, 2) a concept for enhancing OOP robustness by controlling the quality of construction of URM infills leading to passive confinement, 3) experimental investigations of the OOP performance of two full-scale specimens, one with construction flaws commonly found in developing Asian countries and one with proper construction quality, and 4) the proposal and verification of a simple theoretical method based on flexural behavior for evaluation of lateral strength of URM infills. The study neglects the effect of IP-OOP interactions on the OOP performance of the infills. The results of the study will contribute to reducing the effects of potential earthquake disasters on frame buildings with URM infills by providing essential knowledge about the OOP performance of URM infills commonly found in developing Asian countries and an efficient method to improve the construction quality and OOP robustness of URM infills.

2. Characteristics of URM infills and a concept for improving their OOP robustness

As explained in Section 1, because of the improper construction quality of URM infills, improper filling thereby some unintended gaps are present at the top of URM infills. Moreover, buildings are subjected to both IP and OOP forces during an earthquake; thus, the masonry mortar connecting the infill and upper beam/slab is weakened under the IP displacement of the upper beam/slab due to IP forces during an earthquake. Consequently, this phenomenon increases the vertical gaps at the top of the infill. These gaps allow vertical elongation of the infill with crack openings under OOP excitations, making URM infills more vulnerable to OOP collapse, as illustrated in Fig. 2. The main Achilles heel of the URM, i.e., weak flexural tensile strength, allows this behavior. Such gaps at the top can be filled properly with good quality construction practices. Filling the gaps causes confinement and restrains the geometric elongation of the URM infill, which is likely to occur, as illustrated in Fig. 2. In addition, filling the gaps applies passive compression forces on the infill cross section under lateral loads, and these forces restrain the infill wall, as illustrated in Fig. 3. As a consequence of the developed passive compression forces, the tensile forces on the cross section are significantly reduced, and the compressive forces are increased. Since URM infills are strong under compression and weak under tension, the above phenomenon increases the stability and ultimately the OOP robustness of the wall. The basic mechanism of the enhancement of OOP strength is similar to the strengthening mechanism applied by the second author of this paper in a previous study [30].

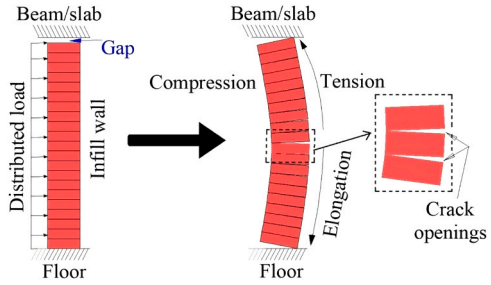

Fig. 2. Failure mechanism of a URM infill with improper filling.

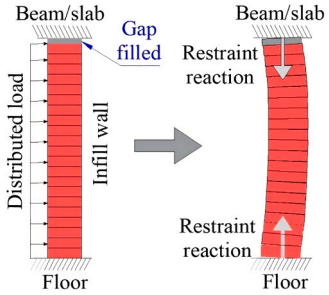

Fig. 3. Mechanism of restraint of a well-constructed URM infill.

3. Experimental program

3.1. Details of the test specimens and materials properties

Two full-scale single wythe (half-brick thick) specimens with running bonds were prepared. Two types of specimens were prepared: 1) a control specimen (specimen CS) that represented URM infills in Bangladesh, characterized by the poor construction practices of URM infills frequently found in developing Asian countries and 2) a well-constructed specimen (specimen WC): constructed in a similar manner to the specimen CS with proper filling at the top. Each specimen was approximately 2000 × 900 × 100 mm in height, length, and thickness, respectively, with 28 layers of burnt bricks (approx. dimensions 200 ×100 ×60 mm in length × width × thickness). Fig. 4 shows details of the specimens. It was difficult to import bricks from Bangladesh to Japan; thus, they were produced in Japan with dimensions and strength similar to those of bricks in Bangladesh [31]. The specimens were constructed in Japan following the same construction practice as those used in Bangladesh.

The bricks were soaked for a sufficient length of time in water and surface-dried before construction to prevent the absorption and seepage of water by and from the bricks. Masonry mortar was prepared by mixing a volumetric cement-to-sand ratio of 1:6, i.e., 1 part by volume of cement to 6 parts by volume of sand, which is a common practice for

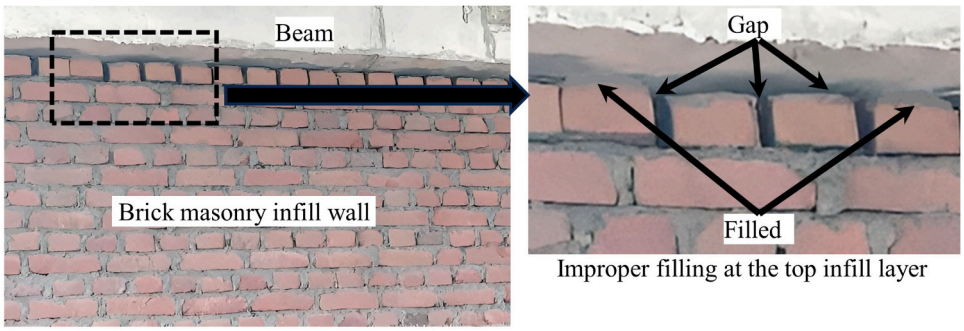

Fig. 1. Improper filling of infill at the top of an infill wall (Nepal).

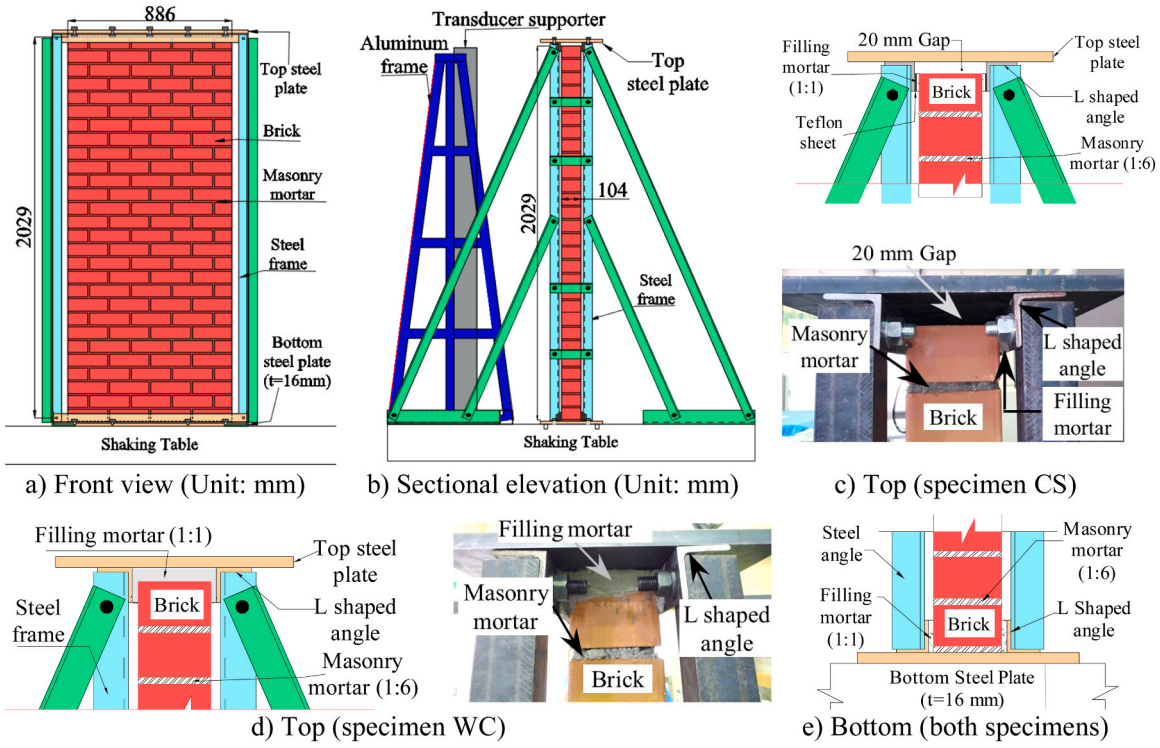

Fig. 4. Details of test specimens.

brick wall construction in Bangladesh. The approximate water-to-cement ratio was 1.3. A steel frame was assembled, and the specimen was constructed on it. The same skilled masons constructed both specimens to represent standard workmanship and ensure construction consistency with a running bond of 10 mm thick masonry mortar. Walls were constructed until the lower half, i.e., up to the 14th layer (approx. 1 m), on the first day, and the remaining upper half was completed on the following day. The height of URM infills varies considerably (less/more than 2000 mm), depending on various factors such as building type, local construction practices and the building topography etc. Hence, the full-scale height of the specimen was adopted as 2000 mm for appropriate representation of the diverse range of infill heights encountered in the practical settings. The specimens simulated part of an infill wall with a full-scale height of 2000 mm and a partially cut length of 900 mm between an RC frame in the surroundings with steel plates at the top and bottom representing upper and lower beams, as shown in Fig. 4. Thus, the effects of columns beside the infill wall were neglected within the test, which might provide a conservative resistance to OOP excitations.

A steel frame was assembled to fix the top steel plate, which was specially designed to provide a fixed end condition at the bottom of both specimens and a roller end condition in the vertical direction for specimen CS (however, a fixed end condition for specimen WC) at the top with no inter-story drift between the top and bottom of the specimens to obtain fundamental experimental data on the effect of passive confinement.

To investigate the material properties, the test samples were prepared from the same material used for the construction of the specimens. Compressive strength tests were conducted on 3 bricks and 3 cylindrical mortar samples with diameters and heights of 50 mm and 100 mm, based on the Indian Standard (IS 3495 (Parts 1–4):1992) [32] and the Japanese Industrial Standards (JIS A 1149:2010) [33] respectively. The investigated mechanical properties of the materials are shown in Table 1. Moreover, to evaluate the flexural strength of the brick wall with 1:6 masonry mortar, five prism specimens with 7 layers of bricks were constructed by the same masons. All prism specimens failed under self-weight during the flexural test, indicating a maximum flexural strength of $\sigma_t = 0.012$ MPa. Hence, due to the lower flexural tensile strength of the brick wall, it was neglected for the lateral strength evaluation in Section 5. The test results summarized in Table 1 were utilized for the lateral resistance evaluation in Section 5.

Table 1
Mechanical properties of materials.

S. N	Description	Average values		Coefficient of variation (%)	
		Compressive strength (N/mm^2)	Density (kN/m^3)	Compressive strength	Density
1.	Brick	14.8	19.7	7.8	0.6
2.	1:6 masonry mortar	1.02	12.7	18.2	7.2
3.	1:1 filling mortar	34.6	20.5	22.1	0.6

3.1.1. Control specimen (specimen CS)

Specimen CS was constructed representing poor construction practices, i.e., improper filling of infills frequently found in developing Asian countries. Because of the improper filling at the top, partial gaps were assumed to be created, as indicated in Fig. 1. Such boundary condition at the top is likely to allow a vertical elongation of the infill, as illustrated in Fig. 2, particularly below the gaps; in contrast, the existence of partial contact areas prevents the horizontal movement of the whole infill. Hence, creating a fixed-end boundary condition at the top of the specimen would overestimate the actual OOP performance of URM infills. On the other hand, there is no complete gap at the top to create the cantilever effect during OOP loading. Thus, idealizing the top end as a roller condition in the vertical direction would be a practical representation of such improper finishing of infills. Consequently, to prevent horizontal slip of the infill on/at the bottom/top steel plates during the experiment, L-shaped angles along the entire length of the specimen were used at both the top and bottom ends. Moreover, for proper slip

restraining, 1:1 filling mortar (with the same volumetric ratio of cement and sand) was used to fill the horizontal gaps between the specimen and the L-shaped angles at both the top and bottom ends, as shown in Fig. 4. Horizontal slip was restrained to prevent cantilever behavior of the specimen, which might occur under a complete gap condition, representing partial filling of mortar between the top layer of the infill and the bottom surface of the upper beam or slab. In addition, Teflon sheets, with negligible frictional resistance, were inserted between the filling mortar and L-shaped angles at the top on both sides, as shown in Fig. 4 c), to prevent vertical friction. Moreover, a vertical gap of approximately 20 mm was kept between the specimen and the top steel plate, as shown in Fig. 4 c), to prevent vertical confinement by the steel frame. To create a fixed support condition at the bottom considering its ease-to-construct even in developing countries, the filling mortar was made directly in contact with the L-shaped angles at the bottom on both sides, as shown in Fig. 4 e). Hence, at the top, a roller condition with freedom in the vertical direction and a fixed support at the bottom end was idealized, as shown in Fig. 23 a). The specific characteristics of specimen WC are described below.

3.1.2. *Well-constructed specimen (specimen WC)*

Specimen WC was constructed in a similar manner to specimen CS. However, in contrast to specimen CS, specimen WC was constructed representing good construction quality of the infills by eliminating the improper filling at the top for specimen CS. For this, the intentionally created top end details in specimen CS to represent an improper construction quality were eliminated. The top vertical gap that represented improper finishing of the infill (as in specimen CS) was filled with 1:1 filling mortar. Moreover, a Teflon sheet was not used between the L-shaped angles and the specimen. Thus, the specimen was in direct contact with L-shaped angles, as shown in Fig. 4 d). The bottom end was kept the same as that of specimen CS, as shown in Fig. 4 e). Hence, both ends of the fixed supports (top and bottom) were idealized as shown in Fig. 23 b). No other arrangement or reinforcement was applied on the specimen other than filling the top vertical gap for proper construction quality.

As explained above, L-shaped angels and filling mortar were utilized to create a proper test setup with controlled and well-defined support conditions at the top and bottom, dismissing other unknown influences on the specimen performance. The test setup contributes to focus on the fundamental response of the infill under lateral loading with well-defined end conditions representing infills with construction flaws and proper construction quality for OOP robustness.

3.2. *Measurement plan*

The experiment was performed by using a 2 × 2 m shaking table at Meiji University, Japan, as shown in Fig. 5, which had a restricted weight of 1000 kg and a maximum acceleration of 8.9 m/s^2. To investigate the OOP performance of the specimens, unidirectional OOP acceleration was applied in the X-direction, as shown in Fig. 5. To monitor the alteration of the specimen response at a macroscopic level in terms of displacement and acceleration, laser displacement transducers (from 1 L to 6 L) and accelerometers (from 1 A to 7 A) were installed at different heights of the specimens, as shown in Fig. 6. The laser transducers were fixed at an aluminum rigid frame that was fixed on the shaking table, as shown in Fig. 6. Moreover, two accelerometers (8 A, X-direction, and 9 A, Y-direction) were fixed on the shaking table to monitor the input accelerations during the excitation. The data recording frequency was 1000 Hz. Fig. 7 shows an overall view of the test setup.

3.3. *Test Program*

A response spectrum was created based on the Bangladesh National Building Code (BNBC) [34] to generate an artificial seismic wave. The design spectral acceleration (S_a) was evaluated using Eq. (1) [34]. The

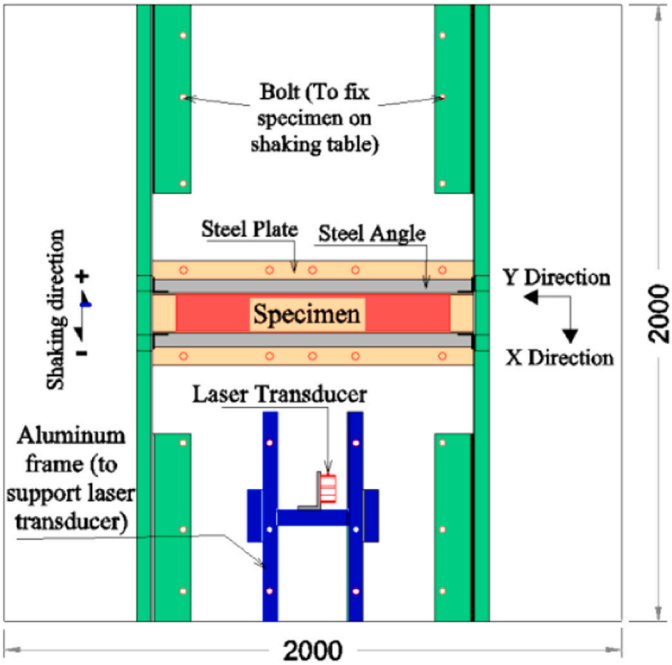

Fig. 5. Arrangement on shaking table (Unit: mm).

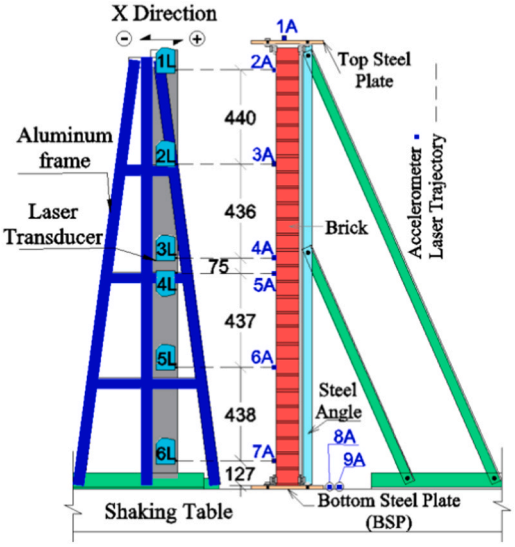

Fig. 6. Measurement detail (Unit: mm).

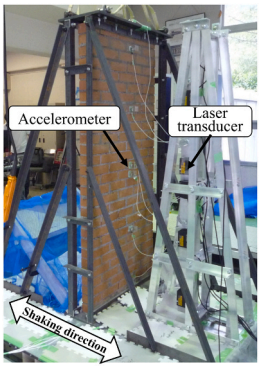

Fig. 7. Test setup.

most severe type of soil, "SD", which represents deposits of loose-to-medium cohesionless soil or predominantly soft-to-firm cohesive soil [34], was considered to create an artificial seismic wave. Fig. 8 shows the normalized acceleration response spectrum (C_s) for the considered soil "SD" for 5 % damping ratio based on BNBC [34]. The artificial seismic wave was generated by using the method suggested by Osaki [35], which defines the phase characteristic of the seismic wave envelope as a function of the assumed earthquake magnitude (M). For this study, the earthquake magnitude (M) was assumed to be 8 by considering the maximum earthquake magnitude that could occur in Bangladesh. Fig. 9 shows the elastic acceleration response spectrum of the artificial ground motion corresponding to the elastic design response spectrum. Fig. 10 shows the artificial seismic wave generated for the experimental investigation. The maximum artificial acceleration was approximately 2.0 m/s^2 (0.2 G). The incremental dynamic tests were performed under 6 input excitations, as summarized in Table 2. The input excitations were gradually increased to investigate progressive damage of the specimen, which also represented the possible ground excitation in Dhaka, Bangladesh.

$$S_a = \frac{2}{3}\frac{ZI}{R}C_s \quad (1)$$

where Z = seismic zone coefficient ($Z = 0.20$, considering the capital city of Bangladesh, Dhaka); I = importance factor ($I = 1.00$, for a common type of building); R = response reduction factor ($R = 1.00$, for elastic condition); and Cs = normalized acceleration response spectrum, which is a function of the soil type and natural period of the building based on the BNBC [34].

4. Experimental results

The experiment was performed 28 days after the specimens were constructed to allow the specimens to develop their full strength. The specimens were carefully lifted at four points via an overhead crane and positioned over the shaking table with bolts. Then, uniaxial shaking was performed in the X-direction as explained in Section 3.3. Each specimen was subjected to a sequence of incremental input excitations, as summarized in Table 2**,** to develop progressive damage until the specimen collapsed or the planned input excitations were completed. Because of the high-frequency noise in the recorded data, a moving average method was used to filter the high-frequency noise, with a frequency of 10 values. Figs. 11 and 12 show the displacement and acceleration profiles of the specimens over their height for each input excitation when maximum values were measured by the laser transducer and accelerometer, respectively. The displacement profiles for specimen CS are shown up to 75 % input excitation since the displacement measurement was limited to 75 % input excitation, as described later in Section 4.1.

The evolution of the hysteretic responses of specimens is illustrated in Fig. 13. To compare the specimen performance, the hysteretic responses were computed in terms of the inertial force (IF) vs. displacement (D) of the brick layer at the mid-height of the specimen (1 m height) monitored by laser transducer, 4 L in Fig. 6. The IF was evaluated by multiplying the acceleration value recorded by accelerometers with a tributary mass associated with the respective accelerometer in the OOP direction based on the previous studies [28,36,37]. The hysteretic responses are shown up to 75 % input excitation for specimen CS (Fig. 13 a)) as explained above. As shown in the figure, during 75 % input excitation, the specimen CS displaced in the negative direction by 11.6 mm, whereas the specimen WC displaced in the positive direction by 5.9 mm. The comparisons with respect to the IF are described in detail in Section 4.3. More detailed behavior of each specimen is explained below.

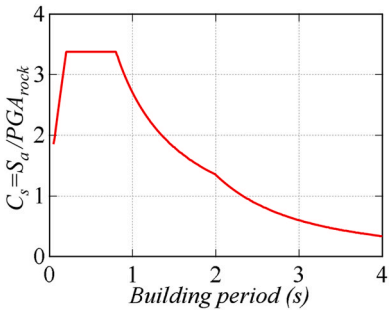

Fig. 8. Normalized acceleration response spectra for soil SD.

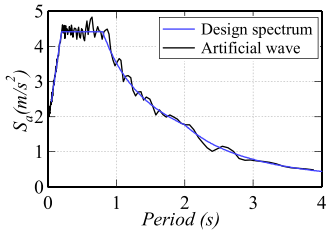

Fig. 9. Elastic acceleration spectrum of artificial ground motion.

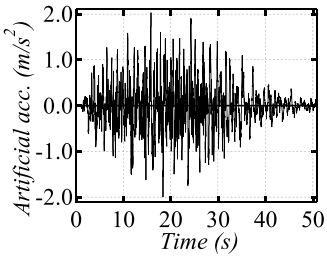

Fig. 10. Artificial seismic wave.

4.1. Specimen CS

Under the first two input excitations, i.e., 10 % (0.2 m/s^2) and 30 % (0.6 m/s^2), the specimen behaved as a rigid body according to visual observation, which was confirmed through the displacement distribution over the specimen height, as shown in Fig. 11**,** and no damage was observed on the specimen. During the third input excitation, i.e., 50 % (1.0 m/s^2), maximum excitement occurred at the mid-height of the specimen in the OOP direction, and the specimen no longer behaved as a rigid body, as shown in Figs. 11 and 12. Moreover, bonding failure was observed between the 1:6 masonry mortar and the topmost brick layer where the confining force due to the self-weight was minimal, decreasing the OOP stiffness. The L-shaped angle was placed at the topmost brick layer, as explained in Section 3.1.1, which restrained the horizontal movement of the top brick layer in the OOP direction. Thus, a permanent sliding displacement of 5 mm was measured during the visual observation, as shown in Fig. 14 **a).** Hence, the plastic hinge was assumed to have formed between the top brick layer and the layer below it. During the 75 % (1.5 m/s^2) input excitation, because of the plastic hinge formed at the top, significant displacement at the top and the sound of falling masonry mortar were observed. Thus, at the end of the excitation, a permanent sliding displacement of 20 mm was measured between the topmost and 2nd brick layers from the top, as shown in Fig. 14 b). Subsequently, the specimen lost its stability; thus, this stage was likely to reach the ultimate state of failure. The specimen was expected to collapse during 100 % input excitation; therefore, displacement measurements (laser transducer) were limited to 75 % (1.5 m/s^2) input excitation. During 100 % (2.0 m/s^2) input excitation, the vertical gap at the top (Fig. 4 c)) caused the specimen to elongate due to the crack opening, as illustrated in Fig. 2. Hence, the permanent sliding

Table 2
Sequence of incremental input excitations.

S. N		1	2	3	4	5	6
Input excitation	% of artificial seismic wave	10	30	50	75	100	125
	Maximum acceleration (m/s^2)	0.20	0. 60	1.00	1.50	2.00	2.50

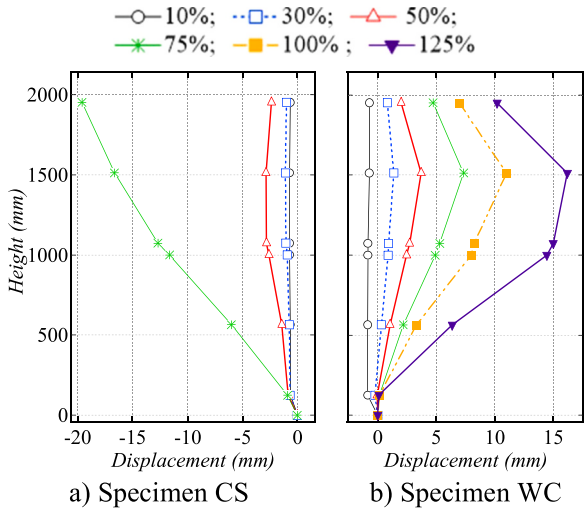

Fig. 11. Displacement profiles of specimens at the time when the maximum value was recorded.

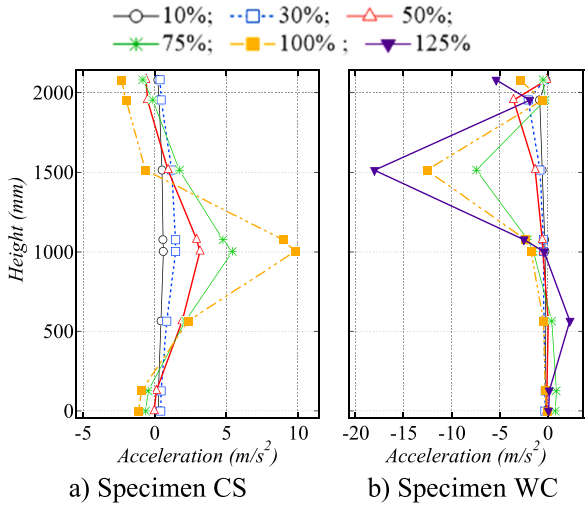

Fig. 12. Acceleration profiles of specimens at the time when the maximum value was recorded.

displacement gradually increased and eventually lost contact between the top brick layer and the layer below it. Finally, the specimen collapsed in the OOP direction, as shown in Fig. 15.

4.2. Performance of specimen WC

While transferring specimen WC to the shaking table, it was subjected to unexpected damage, and a permanent sliding displacement of 5 mm was developed between the topmost brick layer and the layer below it, as shown in Fig. 16. Thus, the specimen was slightly damaged before it was tested. The visual observation and evaluated response of specimen WC revealed that it responded in a similar manner to specimen CS during the first two input excitations, i.e., 10 % (0.2 m/s^2) and 30 % (0.6 m/s^2), in terms of acceleration and displacement, as shown in Figs. 11 and 12. Beyond 30 % input excitation, the specimen no longer behaved as a rigid body, and maximum responses were observed between the top and the mid-height of the specimen, as shown in Figs. 11 and 12.

During 50 % (1.0 m/s^2) and 75 % (1.5 m/s^2) input excitations, a nonuniform response of the specimen in terms of displacement and acceleration was observed, as shown in Figs. 11 and 12. Specimen CS collapsed during 100 % (2.0 m/s^2) input excitation, while specimen WC did not collapse during the same excitation. Thus, for further investigation, an additional input excitation of 125 % (2.5 m/s^2) was applied. During 125 % input excitation, a clear falling sound of masonry mortar was observed. A permanent sliding displacement of 14 mm was observed between the top layer brick and the layer below it, as shown in Fig. 17. The observed permanent sliding displacement (14 mm) during 125 % input excitation was still smaller compared to that of the permanent sliding displacement (20 mm) on specimen CS during 75 % input excitation (Fig. 14 b). Hence, even though specimen WC was damaged prior to the experiment, affecting the anticipated performance, it demonstrated better performance than specimen CS, revealing the positive influence of proper construction quality with passive confinement on improving the OOP robustness. The specimen did not collapse during the shaking table test (up to 125 % input excitation). Thus, to investigate the ultimate capacity, a static tilting test was performed. The static tilting test was a controlled-load test, and the specimen was tilted smoothly and slowly until it collapsed in the OOP direction, ensuring that no forces other than its self-weight acted on it. The tilting angle (α) in Fig. 18 represents an angle of the specimen axis to the horizontal, which specifies the component of the specimen weight acting as a uniform lateral load responsible for the collapse in the tilt direction. While the tilting angle (α) was decreased, the component of the specimen weight gradually increased due to gravitational acceleration. The smaller the tilt angle (α) was, the larger the component of the specimen weight and vice versa. During the test, the tilt angle (α) was monitored with a clinometer, as shown in Fig. 18, until the OOP collapsed. The test was performed by keeping the protruded permanent sliding displacement (Fig. 17) downward, as shown in Fig. 18, to assist the gradual increase in the slide. The specimen collapsed in the OOP direction when the tilt angle (α) was $28^{0,}$ as shown in Fig. 19.

4.3. Replacement to uniform distributed load

The experimental lateral forces acting on the specimens were evaluated in the form of a uniform distribution load (w_{exp}) to evaluate the lateral resistance of the specimens. Linear interpolation was performed to estimate the acceleration between the measured accelerations by assuming a linear acceleration distribution, as shown in Fig. 12. Since the acceleration distribution was not the same over the specimen height, as shown in Fig. 12, the acceleration distribution areas A1-A7 in Fig. 20 were evaluated, and then the total area was divided by the specimen height (H) to evaluate a uniform acceleration distribution (a_{avg}) in Fig. 20. Finally, the uniform lateral load (w_{exp}) acting on the specimen was evaluated by Eq. (2), presuming a uniform distribution of the specimen mass (m) over its height (H). The evaluated time history of the experimental lateral loads during each input excitation is shown in Figs. 21 and 22 for specimens CS and WC, respectively. The evaluated lateral resistance capacity of specimen CS ($_{CS}w$) based on the proposed evaluation methods in Section 5 is shown in Fig. 21. However, the lateral

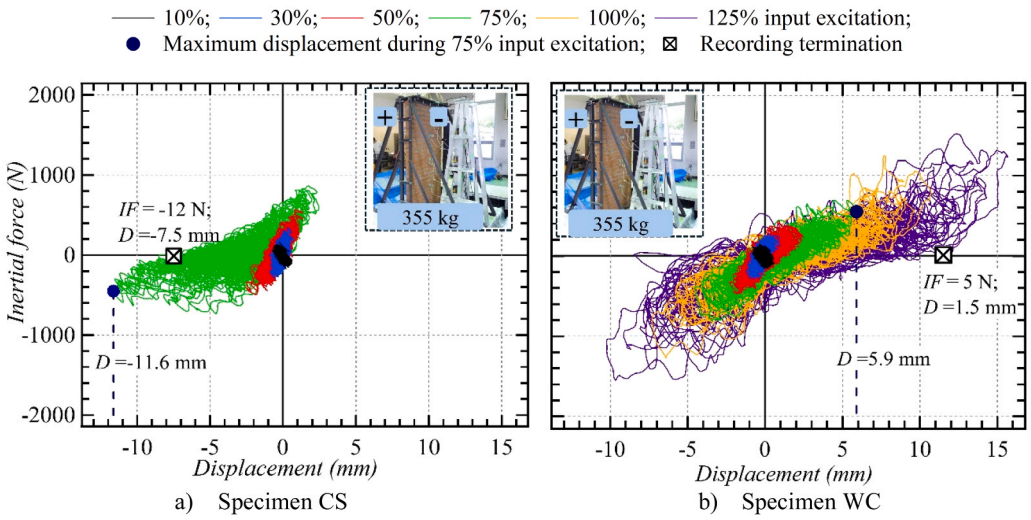

Fig. 13. Inertial force-hysteresis curves.

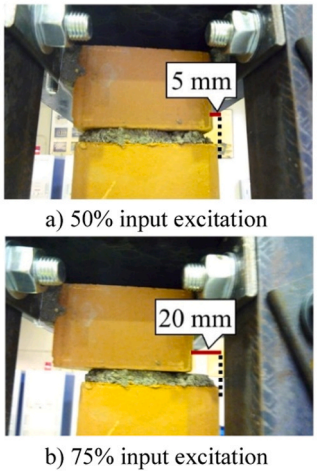

Fig. 14. Permanent sliding displacement on specimen CS.

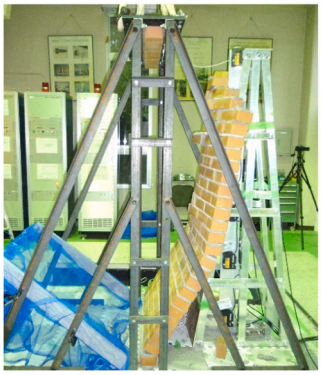

Fig. 15. OOP collapse of specimen CS.

resistance capacity of specimen WC ($_{WC}w$) is not shown in Fig. 22 because of its higher value.

$$w_{\exp} = \frac{m}{H} \times a_{avg} \quad (2)$$

where m= specimen mass (3477 N) and H= specimen height (2029 mm).

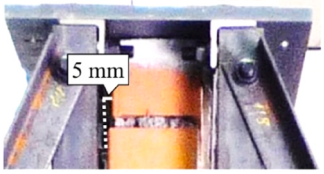

Fig. 16. Initial damage on specimen WC.

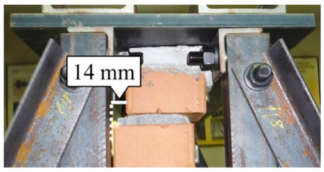

Fig. 17. Permanent sliding displacement of specimen WC (125 %).

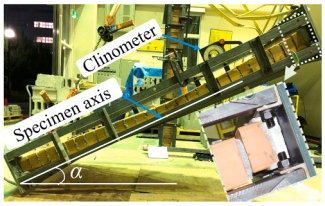

Fig. 18. Static tilting test.

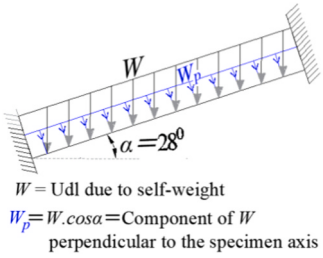

Fig. 19. Forces acting on specimen during tilting test.

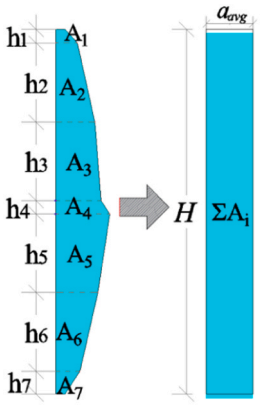

Fig. 20. Evaluation of average acceleration.

During the static tilting test of specimen WC, a uniformly distributed load in the gravitational direction (vertical direction) (W= 1712 N/m) was induced on the specimen due to its self-weight. The OOP force acting on the specimen was the component of W perpendicular to the specimen axis, as explained in **Section 4.2**, $W_p(=W\cos\alpha = 1511$ N/m; $\alpha = 28^0$), as illustrated in Fig. 19. Hence, the ultimate experimental lateral strength of specimen WC was evaluated as $W_p = 1511$ N/m.

5. Proposal of lateral strength evaluation methods

Conservative analytical models for practical applications were proposed to predict the lateral resistance of URM infills with construction flaws (specimen CS) and well-constructed URM infills with passive confinement (specimen WC) based on flexural behavior. The proposed evaluation methods were based on the principle of equilibrium between the acting forces (in terms of the maximum moment (M_m)) and the resistance capacity (in terms of the resistance moment (M_R)). In this study, analytical lateral resistance was evaluated as the capacity of the specimen under idealized end conditions and the forces acting on it. To determine the lateral resistance capacity of the specimen, a uniformly distributed load perpendicular to the specimen axis ($_{CS}w$ for specimen CS and $_{WC}w$ for specimen WC) that represented the capacity of the specimen was assumed to act on each specimen due to the seismic excitation. Fig. 23 shows the bending moment diagram of the specimens along with the maximum moment ($_{CS}M_m$ for specimen CS and $_{WC}M_m$ for specimen WC) under the idealized support conditions as explained in Sections 3.1.1 and 3.1.2.

Fig. 24 shows the forces acting on the cross section of the specimens where the maximum moment (M_m) developed. The resistance moment ($_{CS}M_R$ for specimen CS and $_{WC}M_R$ for specimen WC) was evaluated from the analysis of the cross section utilizing the material properties in Table 1. For the analysis, it was assumed that the plane section would remain plane even after bending. Thus, a linear strain distribution along the specimen cross-section was presumed, and the flexural-tensile strength (σ_t) of the specimen was neglected because of its smaller value (refer to Section 3.1). Finally, the lateral resistance of the specimen (w) was evaluated by relating the maximum bending moment (M_m) and the resistance moment (M_R) of the specimen. Section 3.1 revealed that the masonry mortar has the smallest compressive strength compared to the other constituents of the specimen. Hence, for the performance evaluation, the compressive strength of the 1:6 masonry mortar (σ_M=1.02 N/mm^2) was used for the cross section analysis. Evaluation of the resistance moment (M_R) depended on the resisting mechanism of the specimen and was disparate among the specimens, as explained in the following sections.

5.1. Specimen CS

As shown in Fig. 23 **a)**, the maximum moment (csMm) developed at the fixed support was evaluated using Eq. (3). The resistance moment ($_{CS}M_R$) at the bottom of the specimen where $_{CS}M_m$ was developed was

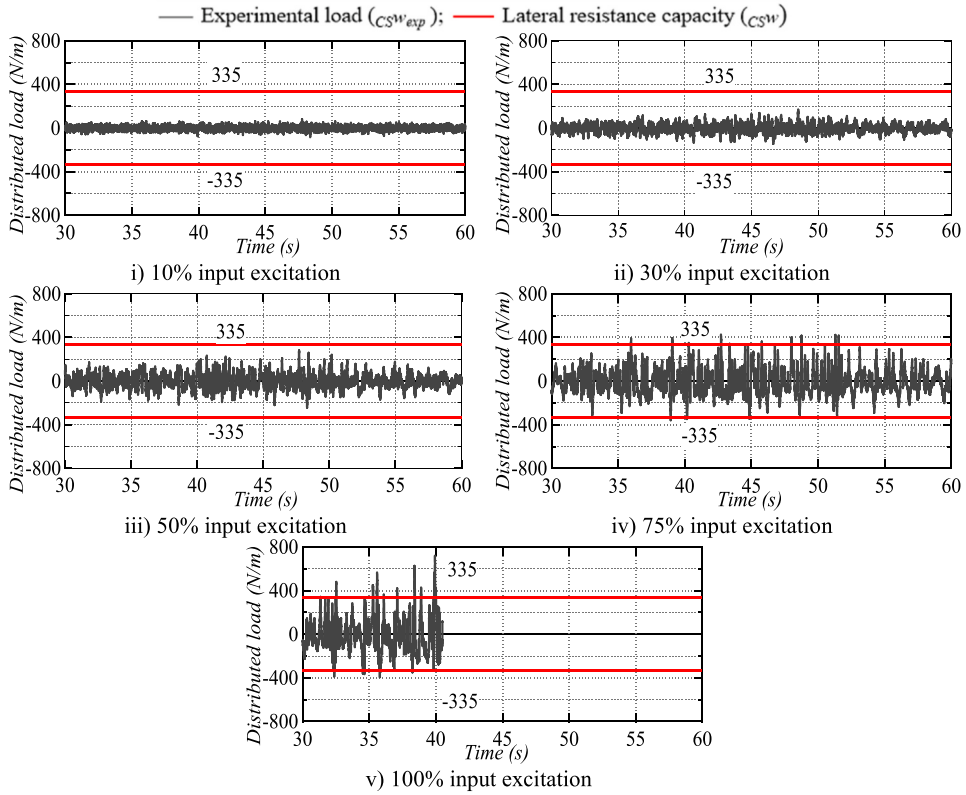

Fig. 21. Comparison of experimental load history and lateral resistance capacity from the proposed method for specimen CS.

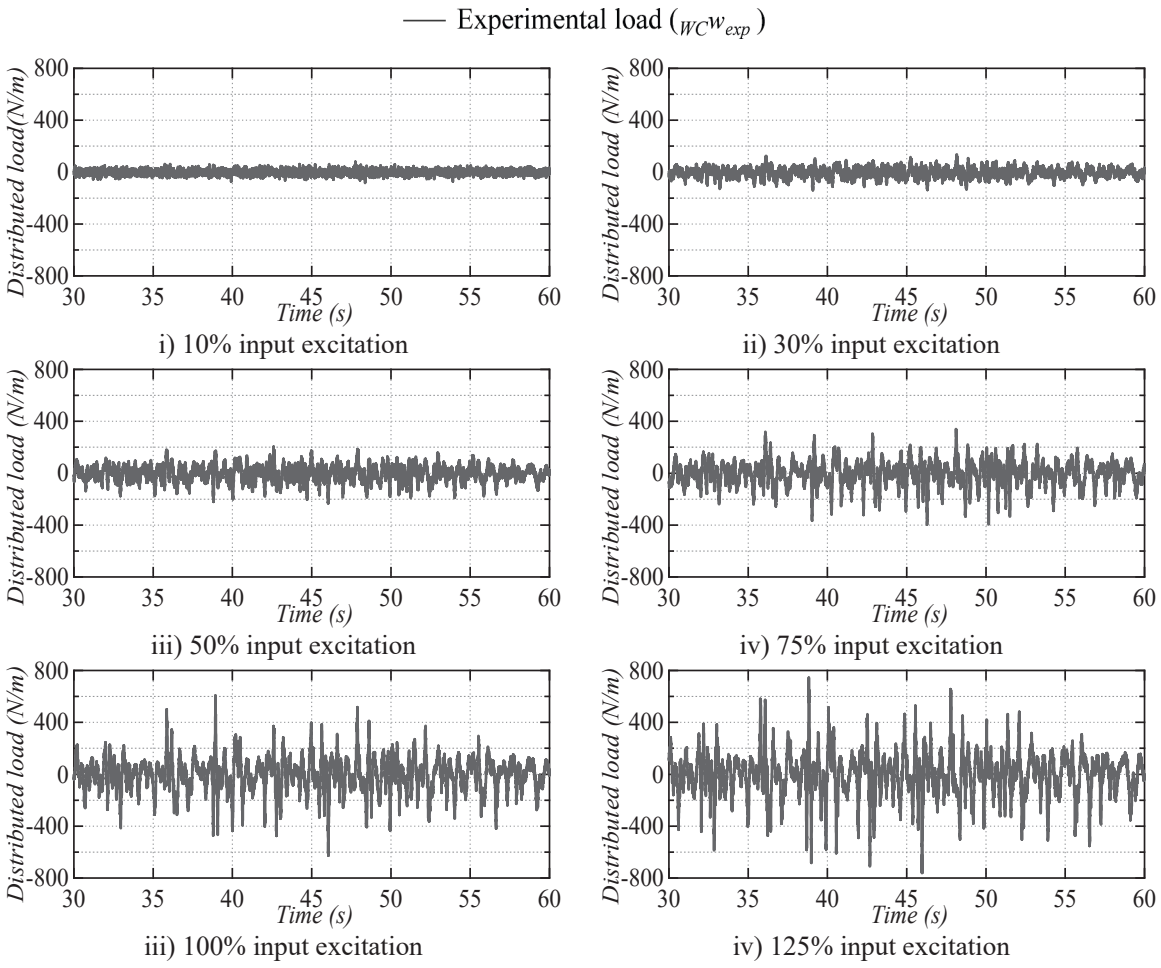

Fig. 22. Experimental load history for specimen WC.

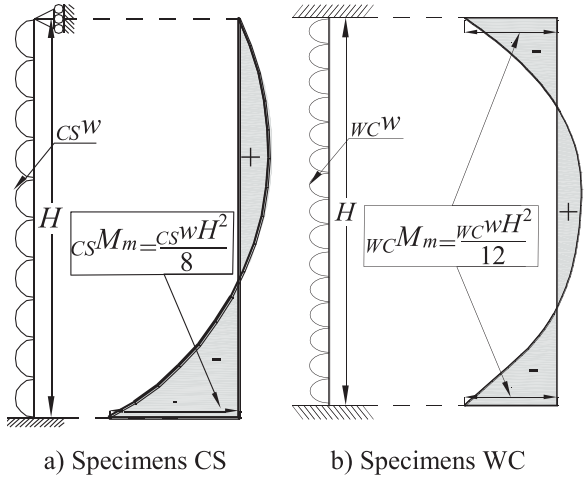

Fig. 23. Bending moment diagram.

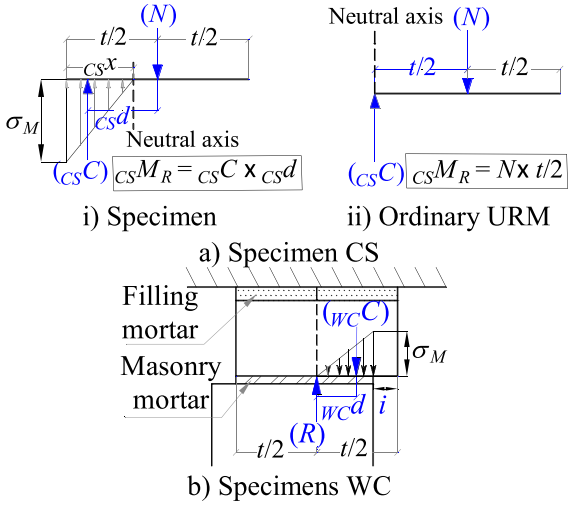

Fig. 24. Action of forces on the specimen.

evaluated using Eq. (4), as shown in Fig. 24 **a) i)** using cross section analysis. The maximum moment ($_{CS}M_m$) should be balanced by the resistance moment ($_{CS}M_R$) for the equilibrium of the specimen; thus, the lateral resistance capacity of the specimen $_{CS}w$ (=335 N/m) was evaluated by using Eq. (5). In this study, the strength of the masonry mortar representing the strength of the specimen was much less compared to the strength of infills in the past studies [3,38]. The infills with higher strength than specimen CS were regarded as ordinary URMs. For ordinary URMs, when the flexural tensile strength was neglected, the depth of the neutral axis considerably decreased. Consequently, the neutral axis nearly coincided at the wall edge, as shown in Fig. 24 **a) ii)**. Hence, the resisting moment ($_{CS}M_R$) was the couple moment developed due to the weight of the wall (N) and the reaction force ($_{CS}C$) at the wall edge. The lateral resistance $_{CS}w$ (=351 N/m) was evaluated by using Eq. (5) as

explained above. For such ordinary URMs, information regarding the dimension and weight of the infill was sufficient to assess the lateral strength, making them practically easy to use.

$$({}_{CS}M_m) = \frac{{}_{CS}w \times H^2}{8} \tag{3}$$

$$({}_{CS}M_R) = {}_{CS}C \times {}_{CS}d \tag{4}$$

$${}_{CS}C = \frac{1}{2}\sigma_M \times L \times {}_{CS}x \tag{4a}$$

$${}_{CS}x = \frac{2N}{\sigma_M \times L} \tag{4b}$$

$${}_{CS}d = t/2 - {}_{CS}x/3 \tag{4c}$$

$${}_{CS}M_m = {}_{CS}M_R \tag{5}$$

$${}_{CS}w = \frac{8 \times {}_{CS}M_R}{H^2} \tag{5a}$$

where t = specimen thickness (104 mm); C = compressive force based on σ_M (1.02 N/mm^2); L = specimen length (886 mm); N = specimen weight (3477 N); ${}_{CS}x$ = neutral axis depth (7.6 mm); and ${}_{CS}d$ = distance. between C and N (104/2 −7.6/3 = 49.5 mm).

5.2. Specimen WC

The maximum moment (${}_{WC}M_m$) developed at the fixed ends, as shown in Fig. 23 b), and it was evaluated using Eq. (6). The possible rotation of the specimen was restrained as the top vertical gap was filled, as explained in Section 3.1. Hence, the passive compression force (${}_{WC}C$) developed during the excitation that restricted the specimen rotation, which was balanced by the restrained force (R), as shown in Fig. 24 b). It was assumed that ${}_{WC}C$ depended on the compressive strength of masonry mortar, as it was the weakest constituent of the specimens (refer to Table 1). Thus, it was presumed that once the masonry mortar failed under compression, the specimen would lose its stability and reach its ultimate stage of failure. In addition, both end fixed support conditions were created as explained in Section 3.1.2; the neutral axis remained at the center of the cross-section at the ultimate stage of failure. Details of the forces acting on the cross section of the specimen at the top end where the confining force due to the self-weight was minimal and the bending moment was maximum are shown in Fig. 24 b). The resistance moment (${}_{WC}M_R$) was evaluated by using Eq. 7. As explained in Section 4.2, permanent sliding displacement (i) of 5 mm and 14 mm were observed on the specimen before the shaking table and static tilting tests, respectively. Hence, considering the permanent sliding displacement (i), Eq. 7 a) and b) were used to evaluate the passive compression force (${}_{WC}C$) and the lever arm length (${}_{WC}d$), respectively. Finally, by relating (${}_{WC}M_m$) to (${}_{WC}M_R$) (Eq. 5), the lateral resistance capacity (${}_{WC}w$) was evaluated analytically as 2016 N/m and 1268 N/m for permanent sliding displacement of 5 mm (shaking table test) and 14 mm (static tilting test), respectively.

$$({}_{WC}M_m) = \frac{{}_{WC}w \times H^2}{12} \tag{6}$$

$${}_{WC}M_R = {}_{WC}C \times {}_{WC}d \tag{7}$$

$${}_{WC}C = 1/2 \times l \times \sigma_M \times (t/2 - i) \tag{7a}$$

$${}_{WC}d = 2/3 \times (t/2 - i) \tag{7b}$$

6. Verification of the proposed Methods

To verify the proposed theoretical evaluation methods in Section 5, the experimental load (w_{exp}) in Section 4.3 was compared with the lateral resistance capacity of the corresponding specimen. Fig. 25 **a)** and **b)** compare the maximum experimental load (w_{exp}) (from Section 4.3) during each input excitation and the evaluated lateral resistance of the corresponding specimen based on the proposed evaluation methods (from Section 5) for specimens CS and WC, respectively.

For specimen CS, during the first two input excitations, i.e., 10 % and 30 %, the maximum experimental load was much less than the resistance capacity ${}_{CS}w$, as shown in Fig. 25 a), which was consistent with the test result that no damage was observed (Section 4.1). During 50 % input excitation, maximum experimental load nearly reached ${}_{CS}w$ (Fig. 25 a)), and a permanent sliding displacement of 5 mm was visually observed, as shown in Fig. 14 a). During 75 % input excitation, maximum experimental load exceeded ${}_{CS}w$ (Fig. 25 a)), resulting in a permanent sliding displacement of 20 mm, as shown in Fig. 14 b), which was congruent with the experimental result, as the specimen seemed to reach its ultimate state. Finally, during the 100 % input excitation, the OOP collapse of the specimen occurred (Fig. 15) after experimental load ${}_{CS}w_{exp}$ responded beyond ${}_{CS}w$ several times, as shown in Fig. 21.

After the 50 % input excitation, the acceleration distribution changed from nearly uniform to nonuniform with greater acceleration toward the mid-height of the specimen, as shown in Fig. 12 a). To investigate the effect of such a nonuniform acceleration distribution on the estimates obtained by the proposed method, the maximum moments at the bottom of the specimen from both the actual (Fig. 12 a)) and the replaced uniform acceleration distributions (Fig. 20) were compared for each input excitation. The maximum discrepancy of 17 % occurred during the 50 % input excitation (the moments at the bottom = 168 N·m and 144 N m under the actual and replaced uniform distribution conditions, respectively, resulting in a discrepancy of (168–144)/144 = 17 %). Hence, the proposed method was confirmed to conservatively estimate the actual OOP resistance capacity of URM infills with construction practices commonly used in developing Asian countries with limited errors.

For specimen WC, the resistance capacity (${}_{WC}w$=2016 N/m) considering the initial permanent sliding displacement of 5 mm is compared with the maximum experimental load in Fig. 25 b). As shown in the figure, the capacity ${}_{WC}w$ from the proposed method was much larger than the maximum experimental load in all input excitations. This was because the maximum experimental load in all input excitations was compared to ${}_{WC}w$ considering the initial damage. Nevertheless, the damage gradually increased for subsequent input excitations, diminishing the resistance capacity. The specimen collapsed during the static tilting test when the experimental load perpendicular to the specimen axis was w_p= 1511 N/m. The evaluated ${}_{WC}w$ was 1268 N/m considering the permanent sliding displacement of 14 mm observed at the beginning of the test. A comparison of w_p= 1511 N/m and ${}_{WC}w$= 1268 N/m showed a small discrepancy of 16 % ((1511–1268)/ 1511 = 16 %). This revealed that had the damage been accounted for, the proposed method would have been more reliable for evaluating the lateral resistance of well-constructed URM infills with passive confinement. It was also found from the experimental and proposed theoretical models that the lateral strength of specimen WC was approximately 5 times higher than specimen CS.

7. Discussion

The study was performed using one specimen for URM infills with common construction flaws and one with proper construction quality by passive confinement. The effects of columns beside the infill were not accounted for within the test. Thus, the proposed methods for evaluation of lateral strength may provide a conservative estimate of lateral resistance. The well-constructed specimen with passive confinement was

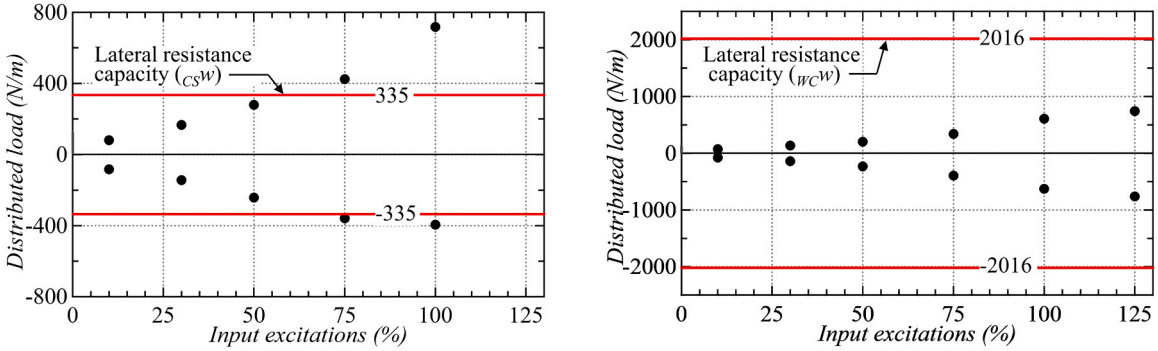

Fig. 25. Comparisons of the maximum experimental loads and lateral resistance capacity from the proposed methods.

subjected to initial damage before the test; thus, the anticipated performance was not acquired. In the future, further investigations will be required to verify the consistency of the investigated results using specimens with different sizes, materials, and details as well as to investigate the effects of the columns beside the infills. In addition, during earthquakes, buildings are subjected to both IP and OOP forces caused by IP drift demands and inertia forces, respectively. IP and OOP interactions represent the phenomenon of degradation of infill performance in one direction due to damage previously accumulated in the orthogonal direction. IP and OOP interaction may affect the OOP performance of URM infill. However, IP and OOP interactions are out of the scope of this study; thus, the effect is not considered in this study. Hence, the effect IP-OOP interaction on the OOP performance of the infill, should be investigated in the future using bi-directional loadings. The experimental and proposed theoretical models revealed that improper construction leads to poor OOP performance, while proper construction quality with passive confinement improves the OOP robustness without any retrofit work. Thus, this study recommends proper construction quality for the URM infill to prevent possible OOP damage.

8. Conclusions

To investigate the impact of passive confinement on the OOP robustness of URM infills, a control specimen with construction flaws representing the common practice for the construction of URM infills in developing Asian countries and a specimen with proper construction quality with passive confinement were prepared. The OOP performance of the specimens was experimentally investigated through shaking table and static tilting tests. Moreover, for the seismic performance evaluation and the safety assessment of URM infills, practical methods for evaluation of lateral strength were proposed and verified. The major findings are summarized below: -

1) The control specimen had a vertical gap at the top representing the improper construction of infills commonly observed in developing Asian countries. A permanent sliding displacement developed at the top of the specimen during 50 % (1.0 m/s^2) input excitation and reached the ultimate state of failure during 75 % (1.5 m/s^2) input excitation. Finally, during 100 % (2.0 m/s^2) input excitation, the specimen collapsed in an out-of-plane direction.
2) A specimen was prepared with proper construction quality with passive confinement. The specimen was damaged before the shaking table test; thus, its anticipated performance could not be obtained during the experiment. However, the specimen survived until 125 % (2.5 m/s^2) input excitation during the shaking table test, and thus, a static tilting test was performed. The specimen collapsed in the OOP direction during the test with a tilt angle of 28^0. Hence, it was experimentally revealed that proper construction quality significantly enhances the OOP robustness of URM infills.
3) A method for the evaluation of the lateral resistance was proposed based on the equilibrium between the resistance moment from a cross-sectional analysis and the maximum bending moment considering the uniform distribution of the external load for both specimens. A nonuniform acceleration distribution was observed after 50 % input excitation for the control specimen. The effects of such a nonuniform acceleration distribution on the proposed strength evaluation were limited to only 17 %. The lateral-resistance of a well-constructed specimen was evaluated considering the permanent sliding displacement observed before the static tilting test. A comparison of the experimental load during the static tilting test and the capacity from the proposed evaluation method showed a small discrepancy of 16 %. Hence, it was confirmed that by considering the construction quality of the URM infill, the proposed evaluation methods can be used to estimate the lateral resistance of URM infills.
4) The poor construction quality of URM infills frequently results in some unintended gaps at the top. The presence of such gaps decreases the OOP strength of the URM infill, making it more vulnerable to OOP collapse. Moreover, this study revealed that proper construction quality by filling such gaps resulted in passive confinement that significantly enhanced the OOP robustness of the URM infill without any specific strengthening by approximately 5 times. This showed the positive effect of passive confinement on the OOP robustness of URM infill walls. Implementation of the investigated method to improve construction quality is characterized by simplicity, cost-effectiveness, and swift execution, and it requires no technical expertise, making it feasible for use in developing countries where URM infills are common. This study also contributed to methods to accurately evaluate the seismic performance of frame structures by assuming the complete IP contribution of URM infills and ensuring the safety of the occupants.

The authors will continue to investigate the OOP performance of URM infills in the future using various URM infills and widen the research field. This expansion of the scope of this research will reinforce the above findings and enhance the seismic performance of RC frame buildings with URM infills.

CRediT authorship contribution statement

Yasushi Sanada: Conceptualization, Funding acquisition, Methodology, Supervision, Writing – original draft, Writing – review & editing, Data curation, Investigation, Resources, Validation, Visualization. **Sujan Pradhan:** Data curation, Formal analysis, Investigation, Writing – original draft, Writing – review & editing, Methodology, Validation, Visualization. **Ho Choi:** Formal analysis, Software. **Yoon Rokhyun:** Resources, Validation. **Kiwoong Jin:** Data curation, Project administration.

Declaration of Competing Interest

The authors declare that they have no known competing financial interests or personal relationships that could have appeared to influence the work reported in this paper.

Acknowledgement

The background data used in this research were supported by the SATREPS project under JICA/JST supervision headed by Prof. Yoshiaki Nakano, the University of Tokyo. In addition, the authors acknowledge the contribution of two graduate students at Osaka University, Mr. Ryuki Hata and Mr. José Tomás D G.

References

[1] Bruneau M, Yoshimura K. Damage to masonry buildings caused by the 1995 Hyogo-ken Nanbu (Kobe, Japan) earthquake. Can J Civ Eng 1996;23(3):797–807.
[2] Okazaki K, Probadi KS, Kusumastuti D, Saito T. Comparison of current construction practices of non-engineered buildings in developing countries. Lisboa: 15WCEE; 2012.
[3] Maidiawati, Sanada Y. R/C frame–infill interaction model and its application to Indonesian buildings. Earthq Eng Struct Dyn 2017;46(2):221–41. DOI: 10.1002/eqe.2787.
[4] Jin K, Choi H, Nakano Y. Experimental study on lateral strength evaluation of unreinforced masonry-infilled RC frame. Earthq Spectra 2016;32(3):1725–47. DOI: 10.1193/100714EQS152M.
[5] Decanini L, Mollaioli F, Mura A, Saragoni R. Seismic performance of masonry-infilled R/C Frames. Canada: 13WCEE; 2004.
[6] Dizhur D, Dhakal RP, Bothara J, Ingham JM. Building typologies and failure modes observed in the 2015 Gorkha (Nepal) earthquake. Bull NZ Soc Earthq Eng 2016;49(2):211–32. DOI: 10.5459/bnzsee.49.2.211-232.
[7] Yatağan S. Damages and failures observed in infill walls of reinforced concrete frame after 1999 Kocaeli earthquake. A/Z ITU J Fac Archit 2011;8 (1)(1):219–28.
[8] Penner O, Elwood KJ. Out-of-plane dynamic stability of unreinfoced masonry walls in one-way bending: Shake table testing. Earthq Spectra 2016;32(3):1675–97. DOI: 10.1193/011415EQS009M.
[9] Vaculik J, Griffith MC. Out-of-plane shaketable testing of unreinforced masonry walls in two-way bending. Bull Earthq Eng 2018;16(7):2839–76. DOI: 10.1007/s10518-017-0282-8.
[10] Sharma S, Tomassetti U, Grottoli L, Graziotti F. Two-way bending experimental response of URM walls subjectd to combined horizontal and vertical seismic excitation. Eng Struct 2020;219:110537. DOI: 10.1016/j.engstruct.2020.110537.
[11] Peng Q, Zhou X, Yang C. Influence of connection and constructional details on masonry-infilled RC frames under cyclic loading. Soil Dyn Earthq Eng 2018;108:96–110. DOI: 10.1016/j.soildyn.2018.02.009.
[12] Erdem MM, Emsen E, Bikçe M. Experimental and numerical investigation of new flexible connection elements between infill walls-RC frames. Constr Build Mater 2021;296:123605. DOI: 10.1016/j.conbuildmat.2021.123605.
[13] Walsh KQ, Dizhur DY, Giongo I, Derakhshan H, Ingham JM. Effect of boundary conditions and other factors on URM wall out-of-plane behaviour: design demands, predicted capacity, and In Situ proof test results. J Struct Eng Soc NZ Inc 2017;30(1):57–81.
[14] Morandi P, Hak S, Milanesi RR, Magenes G. In-plane/out-of-plane interaction of strong masonry infills: from cyclic tests to out-of-plane verifications. Earthq Eng Struct Dyn 2021;51(3):648–72. DOI: 10.1002/eqe.3584.
[15] Di Domenico M, De Risi MT, Ricci P, Verderame GM, Manfredi G. Empirical prediction of the in-plane/out-of-plane interaction effects in clay brick unreinforced masonry infill walls. Eng Struct 2021;227:111438. DOI: 10.1016/j.engstruct.2020.111438.
[16] Milanesi RR, Morandi P, Manzini CF, Albanesi L, Magenes G. Out-of-plane response of an innovative masonry infill with sliding joints from shaking table tests. J Earthq Eng 2022;26(4):1789–823. DOI: 10.1080/13632469.2020.1739173.
[17] Jin W, Zhai C, Zhang M, Liu W, Wei Y, Xie L. Experimental investigation on the in-Plane and out-of-plane interaction of isolated infills in RC frames. Eng Struct 2023;293:116569. DOI: 10.1016/j.engstruct.2023.116569.
[18] Milijaš A, Marinković M, Butenweg C, Klinkel S. Experimental results of reinforced concrete frames with masonry infills with and without openings under combined quasi-static in-plane and out-of-plane seismic loading. Bull Earthq Eng 2023;21(7):3537–79. DOI: 10.1007/s10518-023-01664-4.
[19] Choi H, Nakano Y, Sanada Y, Matsukawa K, Gülkan P, Binici B. Tie system to upgrade out-of-plane performance of infill masonry walls. Earthq Eng Struct Dyn 2024:1–22. DOI: 10.1002/eqe.4096.
[20] Baek ER, Pohoryles DA, Bournas D. Seismic assessment of the in-plane/out-of-plane interaction of masonry infills in a two-storey RC building subjected to bi-directional shaking table tests. Earthq Eng Struct Dyn 2024:1–22. https://doi.org/10.1002/eqe.4109.
[21] Eurocode 6-design of masonry structures–Part 1–1: General rules for reinforced and unreinforced masonry structures. European Committee for Standardization, Brussels; 2005.
[22] FEMA306. Evaluation of earthquake damaged concrete and masonry wall buildings, basic procedures manual. Washington DC: FEMA-306; 1998.
[23] NZSEE 2017. Seismic assessment of existing buildings, Part C: detailed seismic assessment. Wellington, New Zealand 2017.
[24] Gesualdi G, Viggiani LRS, Cardone D. Seismic performance of RC frame buildings accounting for the out-of-plane behavior of masonry infills. Bull Earthq Eng 2020;18(11):5343–81. DOI: 10.1007/s10518-020-00904-1.
[25] Giaretton M, Dizhur D, Ingham JM. Dynamic testing of as-built clay brick unreinforced masonry parapets. Eng Struct 2016;127:676–85.
[26] Graziotti F, Tomassetti U, Penna A, Magenes G. Out-of-plane shaking table tests on URM single leaf and cavity walls. Eng Struct 2016;125:455–70.
[27] Griffith MC, Vaculik J, Lam NTK, Wilson J, Lumantarna E. Cyclic testing of unreinforced masonry walls in two-way bending. Earthq Eng Struct Dyn 2007;36(6):801–21.
[28] Graziotti F, Tomassetti U, Sharma S, Grottoli L, Magenes G. Experimental response of URM single leaf and cavity walls in out-of-plane two-way bending generated by seismic excitation. Constr Build Mater 2019;195:650–70.
[29] Walsh KQ, Dizhur DY, Shafaei J, Derakhshan H, Ingham JM. In situ out-of-plane testing of unreinforced masonry cavity walls in as-built and improved conditions. In: Structures. Elsevier; 2015.
[30] Hayati Y, Sanada Y. Out-of-plane strengthening of masonry walls with passive compression. J Struct Constr Eng 2014;79(702):1193–201. DOI: 10.3130/aijs.79.1193.
[31] Esaki K, Kim S, Suzuki T, Takahashi S, Sanada Y. Compressive test on concrete consisting of brick chip as coarse aggregate. Archit Inst Jpn Tokai Branch Res Rep 2018;56:49–52 (In Japanese).
[32] IS 3495 (Parts 1 to 4). Methods of Tests of Burnt Clay Building Brick. New Delhi, India: Bureau of Indian Standards; 1992.
[33] JIS A 1149. Method of Test for Static Modulus of Elasticity of Concrete. Japanese Standards Association; 2010 (in Japanese).
[34] BNBC. Bangladesh National Building Code, Volume 2, Part 6 Structural Design. Housing and Building Research Institute; 2015.
[35] Osaki N. New. Introduction to Spectrum Analysis of Seismic Motion. Kajima Institute Publishing; 1994 (In Japanese).
[36] Sharma S, Tomassetti U, Grottoli L, Graziotti F. Two-way bending experimental response of URM walls subjected to combined horizontal and vertical seismic excitation. Eng Struct 2020;219:110537. DOI: 10.1016/j.engstruct.2020.110537.
[37] Sharma S, Grottoli L, Tomassetti U, Graziotti F. Dataset from shake-table testing of four full-scale URM walls in a two-way bending configuration subjected to combined out-of-plane horizontal and vertical excitation. Data Brief 2020;31:105851. DOI: 10.1016/j.dib.2020.105851.
[38] Pradhan S, Li Y, Sanada Y. Seismic performance evaluation and risk assessment of typical reinforced concrete frame buildings with masonry infill and conventional vertical extension in Nepal. Bull Earthq Eng 2021. DOI: 10.1007/s10518-021-01246-2.